STRUCTURED LIGHT SCANNING FOR ENDMILL MODELING

Timothy No, Michael Gomez, Ryan Copenhaver, and Tony L. Schmitz
Department of Mechanical, Aerospace, and Biomedical Engineering
University of Tennessee, Knoxville, TN, USA

INTRODUCTION

Multi-axis machining is a cornerstone manufacturing capability for discrete part production. Technology improvements are consistently pursued and implemented to increase productivity and efficiency. This includes new designs for: machines, controllers, spindles, holders, and tools. For endmills, design modifications to the cutting teeth include non-uniform spacing (or pitch), variable helix angle from one tooth to the next and along a single cutting edge, edge honing, and serrated edge geometry, among others. The purpose of these design updates are to affect chip formation and disturb the tooth-to-tooth chip thickness regeneration that serves as the mechanism for self-excited vibration, or chatter, in endmilling operations. While modeling of machining operations has received continuous international attention since the mid-20th century (see [1-3] for comprehensive overviews), relatively less effort has been expended on modeling the behavior of these non-standard geometry endmills, particularly those with serrated cutting edges. Notable exceptions include [4-8].

In this paper, a complete solution for modeling the behavior of non-standard edge geometry endmills is provided. The procedure includes: 1) structured light scanning to produce a solid model of the endmill; 2) identification of the spatial coordinates for the points that define the cutting edges; 3) analysis of those points to extract the cutting edge radius and angle at equally spaced slices along the tool axis; 4) simulation of the cutting force and tool/workpiece deflection using the measured edge geometry; and 5) periodic sampling of the simulation outputs to analyze stability.

SCANNING METROLOGY FOR EDGES

A primary challenge associated with modeling the performance of non-standard edge geometry endmills is that the design details are not generally available. To overcome this obstacle, the reverse engineering capabilities made possible by scanning metrology can be leveraged. One strategy for collecting point clouds from complex surfaces to develop the corresponding solid model is structured light, or fringe, projection. In this technique, a common approach is to project a pattern of parallel lines onto the surface in question. The reflected lines are distorted due to the surface geometry. The measurement system uses the relative positions of the projector and one or more cameras (two cameras is typical) together with the distorted lines to reconstruct the three-dimensional surface. While many commercial options are available, the GOM ATOS Capsule system was used for this research.

The measurements proceeded by first preparing the endmill surface using a removable anti-glare coating and attaching reference targets to the shank surface to enable multiple measurements to be stitched together and generate the solid model. Multiple scans were then completed to obtain the point cloud and 3D model. Figures 1-2 display results for an endmill from Walter Tools (part number 3D1163-6768616). Figures 3-4 present results for a Niagara endmill (part number N68949).

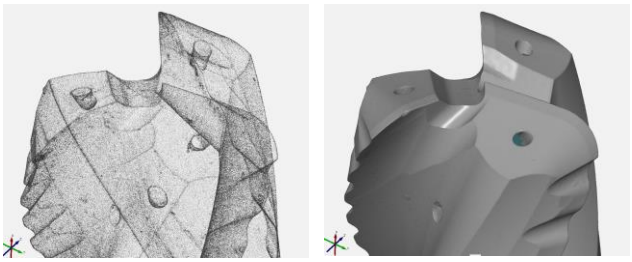

Figure 1. Point cloud (left) and model (right) for Walter Tools endmill obtained from scanning.

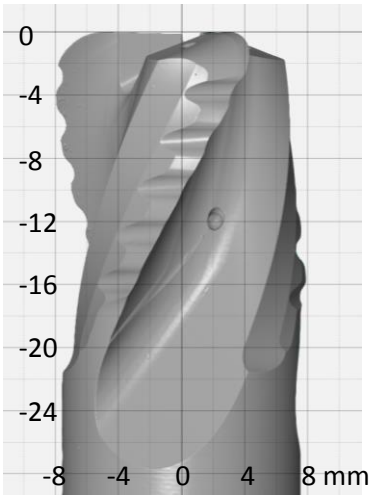

Figure 2. Scale for Walter Tool endmill to visualize edge geometry.

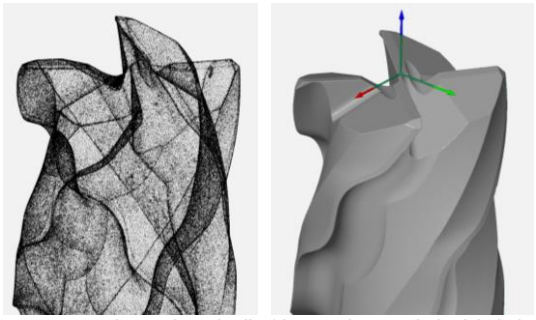

Figure 3. Point cloud (left) and model (right) for Niagara endmill.

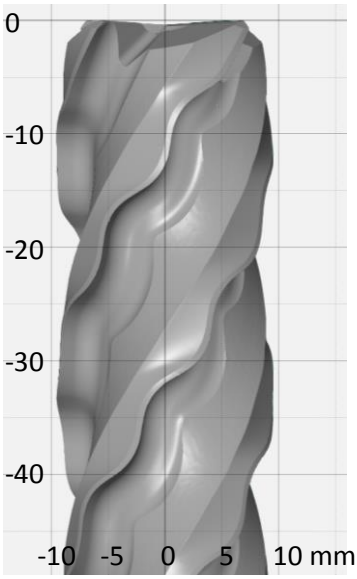

Figure 4. Scale for Niagara 3D model to visualize edge geometry.

The procedure used to extract the edge coordinates from the solid model included four steps.

- First, using the best fit cylinder to the tool shank and the fluted end's extreme point, the origin was established on the tool's center line.
- Second, the points located on the cutting edges were selected. This step required manual manipulation within the GOM software. In function, it was analogous to updating driving directions in Google Maps by dragging the original route to new roads.
- Third, the radius, r, and angle, ϕ, for each edge point was calculated. The teeth angles were normalized to a selected tooth and constrained to values between 0 and 360 deg; the z value (tool axis) was retained to obtain a triplet, {r, ϕ, z} for each point.
- Fourth, because the point density was higher than required for the time domain simulation, linear interpolation was used to obtain the triplet for axial slices located every 0.1 mm over the full flute length; see Fig. 5, which shows the origin, edge points, and axial slices for the Walter Tool endmill.

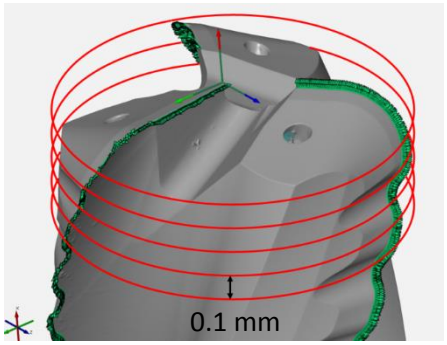

Figure 5. Cutting edge points and axial slices (not to scale) for linear interpolation. The origin is also identified (Walter Tool).

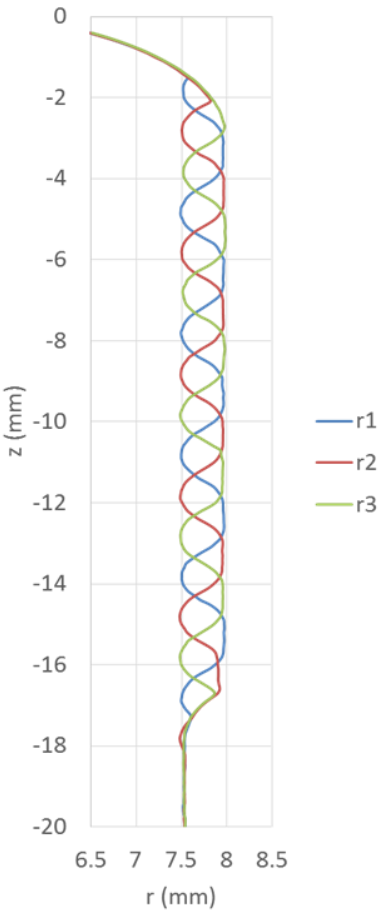

Figure 6. Radius value at each axial slice for all three endmill teeth (Walter Tool).

Example radius results for the Walter Tool endmill are provided in Fig. 6. It is observed that the specialized tool geometry incorporates large radius variation along the cutting edge and that these radius variations are phased from one tooth to the next (120 deg spacing between the peaks for the three teeth). For each tooth the angle variation from the nominal helix, $\Delta\phi$, was not significant. The mechanism for increased stability with this design is, therefore, the segmentation of the cutting edge into bands using the radius variation. This effectively reduces the axial depth of cut, while simultaneously increasing the chip thickness. Also, the point cloud data was used to determine the macro-geometry: 8 mm shank radius, 28.3 deg helix angle, and 2.785 mm bull nose radius.

Angle results for the Niagara endmill are provided in Fig. 7, where the angle variation is periodic and progressively offset by 90 deg between teeth. There is no appreciable radius variation in this case. The mechanism for increased stability with this design is, therefore, disruption of regeneration from one tooth to the next by the variable pitch. The point cloud data was used to determine the macro-geometry: 9.5 mm shank radius and 35.1 deg helix angle.

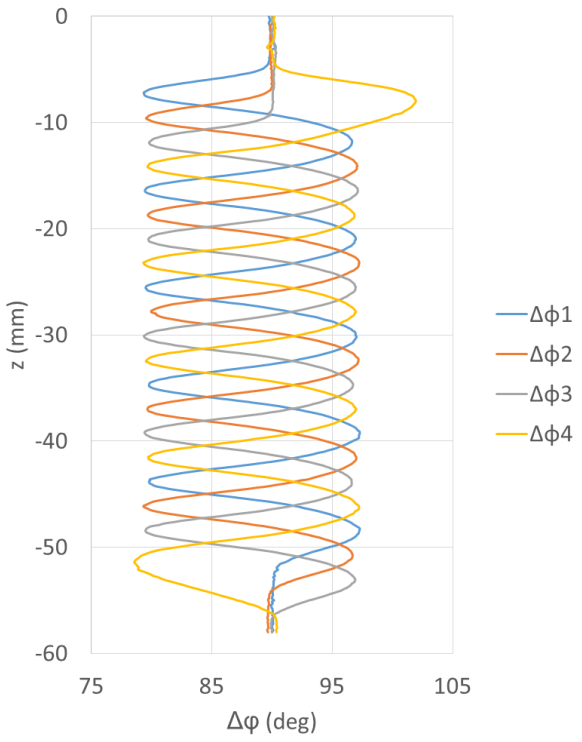

Figure 7. Deviations of teeth angles from nominal helix (Niagara).

TIME DOMAIN SIMULATION

Time domain simulation enables numerical solution of the coupled, time-delay equations of motion for milling in small time steps [1]. It is well suited to incorporating the inherent complexities of milling dynamics, including complicated tool geometries (runout, or different radii, of the cutter teeth, non-uniform teeth spacing, and variable helix) and the nonlinearity that occurs if the tooth leaves the cut due to large magnitude vibrations. The simulation applied here is based on the regenerative force, dynamic deflection model described in [1]. As opposed to analytical or semi-analytical stability maps that provide a global picture of the stability behavior, time domain simulation provides information regarding the local cutting force and vibration behavior for the selected cutting conditions. The simulation used in this study is described in the following paragraphs.

The strategy used to model the large radius variation for each tooth on the Walter Tool endmill (Fig. 6) was to define a nominal tooth shape with no serration and then incorporate the radial deviation as runout. It is observed in Fig. 6 that tooth 3 follows the nominal bull nose profile up to the shank diameter. The tooth 3 geometry was therefore selected as the reference up to -2.4 mm. The radius was set to a constant value of 7.974 mm (i.e., the value at -2.4 mm) for *z* values of -2.5 mm and beyond. The runout was then determined for each tooth as the difference between the reference profile and the actual radius value at each *z* interval. The peak-to-peak variation was 0.48 mm. For the Niagara endmill, the runout was small, but the intentional *z*-dependent pitch was incorporated by specifying the tooth angle at each *z* location using the interpolated data from the 3D model edge identification.

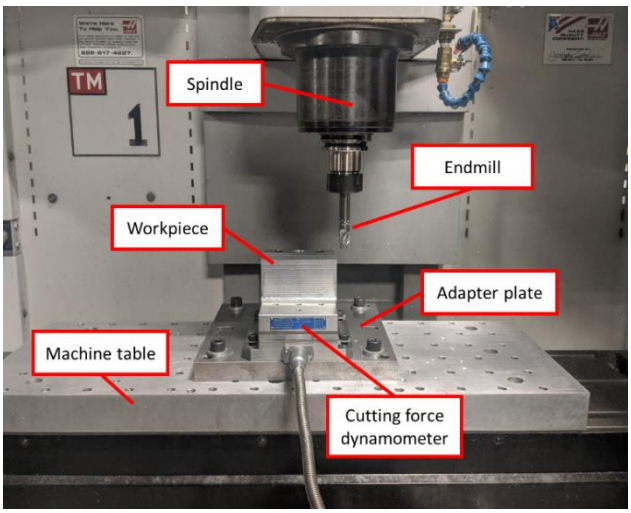

Figure 8. Experimental setup for milling force measurement.

EXPERIMENTAL SETUP

The experimental setup for milling force measurement is shown in Fig. 8. Trials were completed on a Haas TM-1 three-axis computer numerically controlled (CNC) milling machine. The 7075 aluminum workpiece was mounted on a cutting force dynamometer (Kistler 9257B) and the endmill was clamped in a collet holder and inserted in the CAT-40 spindle interface. For the Walter Tool endmill, tests were performed at axial depths of cut from 4 mm to 14 mm. The commanded feed per tooth for these down (climb) milling experiments was 75 µm/tooth, the spindle speed was 4000 rpm, and the radial depth of cut was 2 mm (12.5% radial immersion). The tool and workpiece frequency response functions, or FRFs, were measured by impact testing, where an instrumented hammer is used to excite the structure and the response is measured using a linear transducer (a low-mass accelerometer for this research). These were used in the simulation.

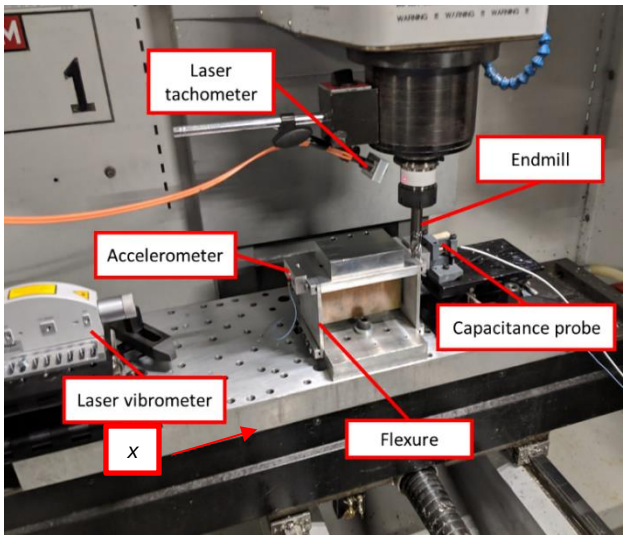

Figure 9. Experimental setup for stability testing.

For the Niagara endmill, tests were performed at axial depths of cut from 5 mm to 25 mm. The commanded feed per tooth for these down (climb) milling experiments was 100 µm/tooth, the spindle speed was 300 rpm, and the radial depth of cut was 1.9 mm (10% radial immersion). The FRFs were again measured and the modal parameters were extracted for use in the time domain simulation.

The setup for the Walter Tool endmill stability testing was similar to Fig. 8, but the aluminum alloy workpiece was mounted on a parallelogram, leaf-type flexure rather than the dynamometer (the flexible direction for the flexure was oriented parallel with the machine's *x* direction); see Fig. 9. Note that the workpiece (flexure) *x* direction was significantly more flexible than the tool or flexure *y* direction.

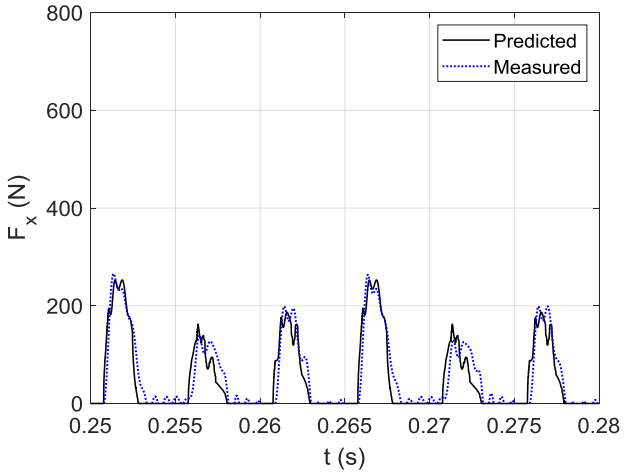

Figure 10. Measured and predicted force for b = 4 mm (Walter Tool).

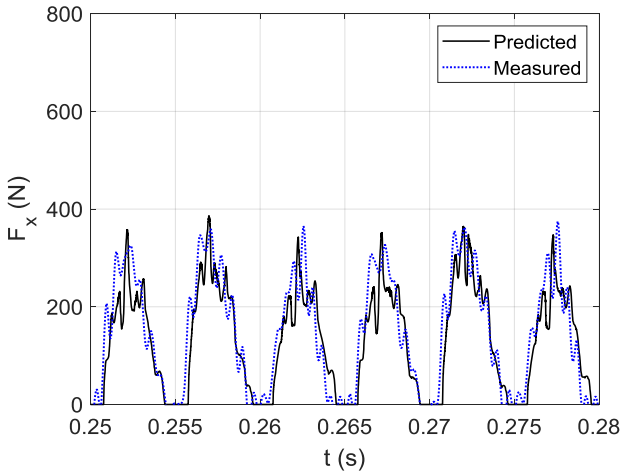

Figure 11. Measured and predicted force for b = 14 mm (Walter Tool).

RESULTS

Forces for Walter Tool endmill

Measured and predicted feed direction force values, F_x, for b = 4 mm and 14 mm are shown in Figs. 10-11. Good agreement is observed, although the dynamometer's structural dynamics added oscillations to the measured force. It is seen that the force progresses from a smoother profile while engaged in the cut for b = 4 mm to highly discontinuous at b = 14 mm. This is the result of the tool design which cuts with approximately 1 mm wide "bands" of limited axial depth, where the local radius is close to the shank diameter. These bands are separated on each cutting edge by the approximately 2.5 mm spatial period of the radius

variation along the tooth helix (see Figs. 2 and 6). As the axial depth increases, more bands are individually engaged (with a larger than commanded chip thickness) and the force is subsequently increasingly discontinuous even though all cuts are stable (forced vibration only).

Forces for Niagara endmill

Measured and predicted feed direction force values for *b* = 5 mm and 20 mm are shown in Figs. 12-13. As shown in Figs. 4 and 7, the spatial period for the pitch angle variation is approximately 10 mm. The force profile progresses from a typical down milling signal for *b* = 5 (Fig. 12), where the pitch angle variation is not fully incorporated, to nearly constant at *b* = 20 mm (Fig. 13), where two full spatial periods are engaged.

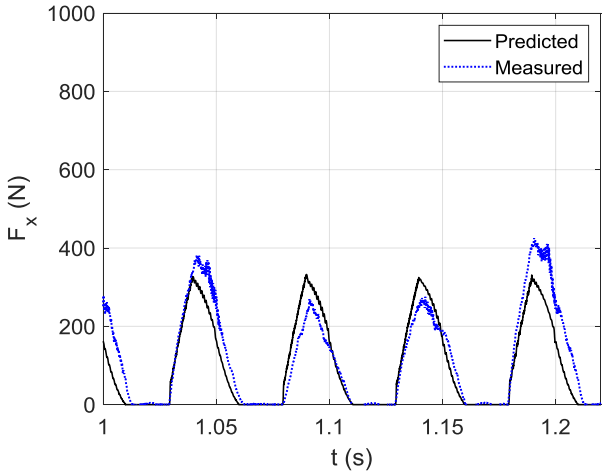

Figure 12. Measured and predicted force for b = 5 mm (Niagara).

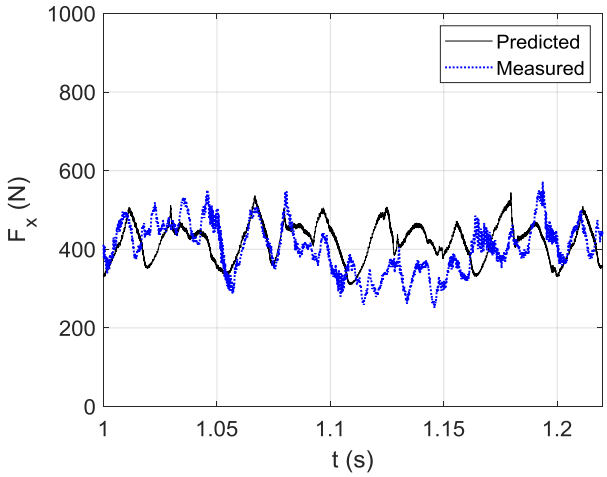

Figure 13. Measured and predicted force for b = 20 mm (Niagara).

Stability prediction and validation for Walter Tool endmill

Given the validated force results, stability testing was completed using the Fig. 9 setup. Workpiece (flexure) displacement and velocity predictions were generated using the time domain simulation. The down milling radial depth of cut was 3 mm and the commanded feed per tooth was 100 μm/tooth for all tests.

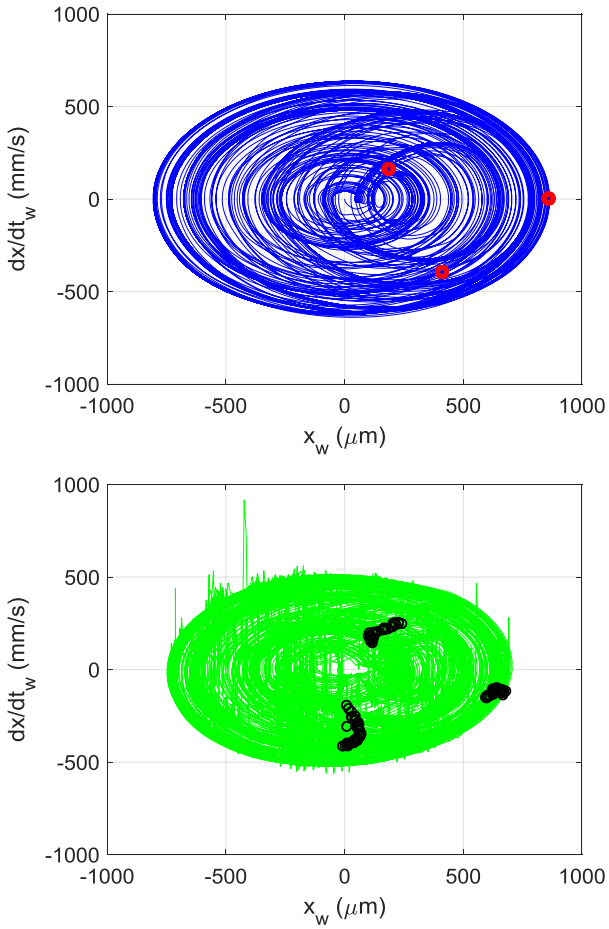

Figure 14. Poincaré maps for period-3 bifurcation at {2750 rpm, 10 mm}. (Top) predicted. (Bottom) measured. The local jumps in measured velocity are due to chips passing through the laser beam.

To establish stability, the workpiece *x* direction displacement and velocity signals were sampled once per revolution (i.e., at the spindle rotating frequency) [9]. The laser tachometer shown in Fig. 9 was used to generate the sampling signal. This periodic sampling approach was used to determine if the milling response was synchronous with the spindle rotation (or not) by constructing Poincaré maps (i.e., the periodically sampled displacement

was plotted versus the periodically sampled velocity) for both experiment and prediction. To interpret these Poincaré maps, if the cut is stable (i.e., it exhibits forced vibration only), the data repeats with each spindle revolution and the sampled points appear at one location. If self-excited vibration (i.e., regenerative chatter, or secondary Hopf bifurcation) occurs, however, an elliptical distribution of sampled points is observed due to the presence of both the (generally) incommensurate chatter frequency and the tooth passing frequency (and its harmonics). Additionally, period-*n* bifurcations can occur, where *n* represents the number of periods between repetition. A period-3 bifurcation, for example, exhibits motion that repeats every three rotations. Results are presented in Figs. 14-15 for two spindle speed-axial depth combinations, where the once-per-revolution samples (circles) are superimposed on the continuous *x* direction workpiece displacement, x_w, and velocity, dx/dt_w. Good agreement is observed in each case.

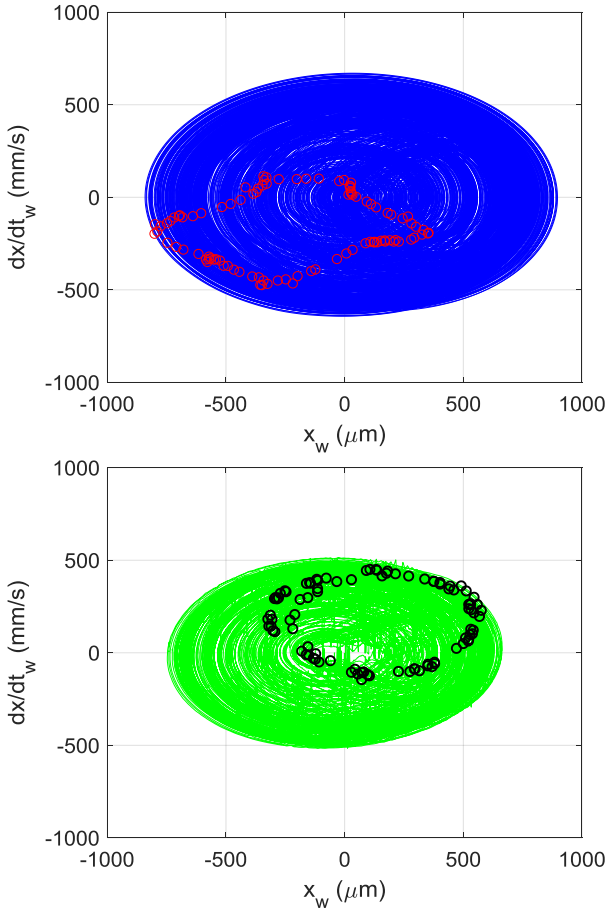

Figure 15. Poincaré maps for fully developed regenerative chatter (secondary Hopf bifurcation) at {2850 rpm, 10 mm}. (Top) predicted. (Bottom) measured.

CONCLUSIONS

This paper provides a reverse engineering solution for modeling the behavior of non-standard edge geometry endmills. Structured light scanning was used to produce a solid model of two different endmills. From these models, spatial coordinates for the points that define the cutting edges were extracted. The points were used to determine the cutting edge radius and angle at equally spaced points along the tool axis. The cutting edge geometry was then incorporated in a time domain simulation that was used to predict cutting force and tool/workpiece deflection for user-selected operating parameters.

ACKNOWLEDGEMENTS

This material is based on work supported by the National Science Foundation under Grant No. CMMI-1561221.

REFERENCES

[1] Schmitz, T.L. and Smith, K.S., 2009, Machining Dynamics: Frequency Response to Improved Productivity, Springer, New York, NY.

[2] Altintas, Y., 2012, Manufacturing Automation: Metal Cutting Mechanics, Machine Tool Vibrations, and CNC Design, Cambridge University Press.

[3] Altintas, Y. and Weck, M., 2004, Chatter stability of metal cutting and grinding, CIRP Annals-Manufacturing Technology, 53/2: 619-642.

[4] Wang, J.-J. and Yang, C.S., 2003, Angle and frequency force models for a roughing end mill with a sinusoidal edge profile, International Journal of Machine Tools and Manufacture, 43: 1509-1520.

[5] Merdol, S.D. and Altintas, Y., 2004, Mechanics and Dynamics of Serrated Cylindrical and Tapered End Mills, Journal of manufacturing Science and Engineering, 126: 317-326.

[6] Dombovari, Z., Altintas, Y., and Stepan, G., 2010, The effect of serration on mechanics and stability of milling cutters, International Journal of Machine Tools and Manufacture, 50: 511-520.

[7] Grabowski, R., Denkena, B., and Köhler, J., 2014, Prediction of process forces and stability of end mills with complex geometries, Procedia CIRP, 14: 119-124.

[8] Tehranizadeh, F., and Budak, E., 2017, Design of serrated end mills for improved productivity, Procedia CIRP, 58: 493-498.

[9] Honeycutt, A. and Schmitz, T., 2017, Milling stability interrogation by subharmonic sampling, Journal of Manufacturing Science and Engineering, 139/4: 041009.